Evaluation of surface profiles of sloped pockets machined on Si_3N_4-TiN via micro-EDM milling

ICOMM 2014 No.

F. Modica[1], V. Marrocco[1], G. Guadagno[1] and I. Fassi[2]

[1] *ITIA-CNR, Institute of Industrial Technology and Automation, National Research Council, Via P. Lembo 38/F, Bari, Italy*
[2] *ITIA-CNR, Institute of Industrial Technology and Automation, National Research Council, Via Bassini 15, Milano, Italy*

Abstract

In this paper, the study of tridimensional 45°-sloped pockets realized in Si_3N_4-TiN ceramic composite machined via micro-EDM milling is reported. The experimental results obtained by measurements performed directly on the micro-EDM milling machine show that most of the errors of the inclined surface manufacturing are detected in the first part of the erosion process. Our analysis shows that the surface imperfections are related to the energy used in the process, the frequency of electrical touches done to detect tool wear and feature depth error, the initial values of the parameter set to compensate tool wear and the layer thickness set to implement the layer-by-layer strategy. Morphological measurements, performed using Axio CSM 700 confocal microscope, have confirmed that the surfaces of the inclined walls suffer of some defects on the top of the pockets. However, the surface profiles are quite good and no step-like trends have been detected.

Keywords: silicon nitride, micro-EDM, micro-feature, draft angle.

1. Introduction

Silicon nitride-based ceramics [1][2] are employed as engineering materials in high-temperature applications, in aggressive environments, such as the production of micro-injection moulds, ceramic glow plugs, igniters, ceramic heaters and also for load bearing prostheses and bone mini-fixation devices as biocompatible materials. However, due to their high hardness and brittleness, the production of complex shapes from simple pieces of silicon nitride via conventional mechanical machining is difficult and expensive in terms of cost and times. Ceramic composites can be synthetized by incorporating an electrically conductive reinforcement in the original structure, such as particles of WC, $MoSi_2$, TiN, TiC, TiCN, TiB_2 and ZrN, over about 30 vol%, which turns ceramics into electro-conductive composites suitable to be manufactured by electrical discharge machining (EDM). Micro-EDM [3][4] allows to machine micro-sized features in conductive materials regardless to their hardness, strength or brittleness. However, the texturing of such ceramic composites is by no means an easy task, since the assessment of micro-EDM process parameters able to guarantee small features, high accuracy, precision and desired surface roughness demands a wide experimental campaign to be done. Moreover, due to chemical reactions triggered by the thermal process, the surface quality of ceramic composite devices is typically affected by layer recast, heat affected zone, debris deposition and re-solidification of particles. Several experiments carried out on SiC, B_4C and Si_3N_4-TiN [5][6][7] show that some problems arise during the erosion process because of the occurrence of a small transition zone between stable and unstable machining, which is typical for low electrically conductive materials. In order to obtain a good surface planarity and reduced depth errors, tool wear compensation is mandatory. Since the material removal process involves both tool and workpiece, the tool is subjected to a modification, both in length and side, and induces a consequent variation of the actual depth and shape of the machined micro-features. Usually, in order to manage tool wear, wear compensation strategies are adopted [8][9]. For our micro-EDM machine, SARIX SX 200, the parameter ascribed to the compensation of the longitudinal tool wear rate calculated with respect to the tool path covered is referred as adjustment factor. This parameter is updated via a procedure comprising a number of electrical touches done at a reference point located on the workpiece to check the tool wear rate along with the depth error and the adjustment factor update during each machining process. The increase of such control touch number proved to be as a simple as an effective procedure to obtain reliable tool wear estimation and reduce depth error values [9][10]. This technique has been also adopted to perform the experiments proposed in this paper. The preliminary study about the limits encountered in manufacturing of Si_3N_4-TiN micro-features has been already presented in [11]. In that study, micro-pins machined via micro-EDM milling have been realized with the goal of exploring the minimum achievable micro-feature size indispensable to create a texturing to be exploited in biocompatible micro-implants. The results showed that a fine machining is strictly dependent on the energy level and tool diameter adopted during the process.

In this paper, we intend to extend the study relating to the micro-EDM milling of Si_3N_4-TiN features to the next step. Indeed, preliminary experiments concerning 3D freeform features are reported. In particular sloped pockets having a draft angle equal to 45° on Si_3N_4-TiN samples are machined. This geometry allows the direct evaluation of depth errors, of geometrical profiles and of surface defects. Two energy levels and a standard tool (nominal diameter equal to 0.4 mm) are used to machine the pockets. The effects on depth error of energy level, layer thickness (used for the layer-by-layer strategy implementing the micro-EDM milling machining), the number of electric touches (control number) and the initial value of the tool wear compensation factor (called adjustment

factor) are considered in this analysis. Additional geometrical measurements show that a good surface and draft angle accuracy can be accomplished by the machining process.

2. Sloped pockets machining and measurements

2.1. Micro-EDM machine set up

Sloped pockets (pyramids) having draft angles equal to 45° have been manufactured on Si_3N_4-TiN ceramic samples using a Sarix SX 200 micro-EDM machine (Fig. 1). The samples have been synthetized by ISTEC-CNR. The draft angle has been defined with respect to the Z axis and the depths are equal to 1 mm.

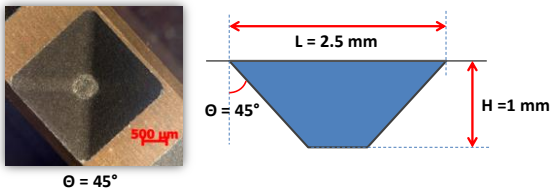

Fig. 1: A machined sloped pocket (left) and a sketch identifying the geometrical parameters (right).

The tool is a tungsten carbide (WC) cylindrical rod having negative polarity and nominal diameter equal to 0.4 mm. The workpiece is positively polarized. The dielectric used for the flushing is a hydrocarbon oil. The micro-EDM milling of the sloped pockets has been implemented adopting the layer-by-layer strategy. In this analysis, some process parameters (energy levels, layer thickness, LT, control number, CN, adjustment factor, Adj) are varied to investigate their effect on the surface defects of the inclined planes. For each considered parameter combination, all experiments have been randomized and three replica have been done for better result accuracy and reliability (Table 1). Fig. 2 reports the scheme of the machined pyramids and the location of the replica in the sample.

Table 1: trials and related parameters.

	E	LT	CN
PYR1	110	2	100
PYR2	110	2	50
PYR3	110	2	25
PYR4	110	1	100
PYR5	206	5	50
PYR6	206	5	25
PYR7	206	2	100
PYR8	206	2	50
PYR9	206	2	25

Two energy levels, indicated by the indexes E110 and E206, have been chosen for finishing and roughing regimes, respectively. In order to ensure stability of the erosion process and flatness of the machined surfaces, the layer thicknesses chosen in all experiments have values ranging from 1 to 5 µm. In order to estimate the depth error and tool wear during machining, electrical touches are systematically performed in a determined point located in the workpiece surface, called control point. This procedure is repeated a number of times set by the end-user, namely the control number (CN).

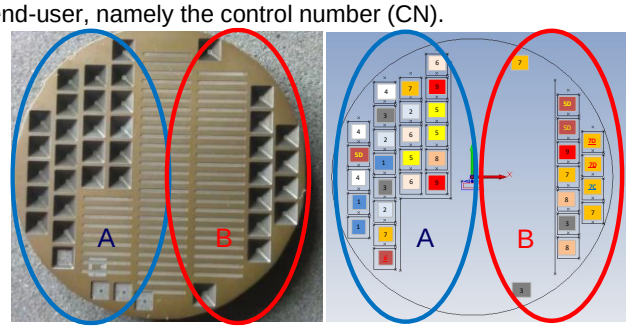

Fig. 2: Samples with machined features and scheme of the pyramid locations: all replica are evidenced and two different areas (A and B) of the samples are highlighted to stress the observed material inhomogeneity.

The parameter responsible of the tool wear compensation operated with respect to the path covered by the tool is called adjustment factor. Since the tool wear varies during the machining, this factor is updated during these control touches according to the tool wear measurement. In order to mitigate the influence of measurement error of the tool length the adjustment factor is updated considering the last five measurements. Typically, the increase in control number value has good effect on depth error, making it comparable to the accuracy of the machine axes. Some additional control touches are also introduced between two subsequent standard control touches implemented in each part program. This fact could induce some effects on the repeatability: the tool is displaced from the erosion point to the control point several times. However, these additional measurements underline interesting aspects about the tool path effects, as highlighted in the following parts.

2.2. Evaluation of machining errors and feature surface profiles.

The experimental results are evaluated adopting two kinds of measurements. The first one derived from the electric touches performed on the Sarix SX 200. The electrical touches are uniformly distributed with respect to the cavity depth and their number is indicated by the control number (CN). These measurements esteem the profile error of the sloped surface by a punctual measure of the tool length and then they cannot observe local effect on a single surface. The second set of measurements is obtained by Axio CSM 700 confocal microscope using a resolution of 2.5µm. An example of the feature acquisition is reported in Fig. 3. The acquired images are then post-processed in order to evaluate the surface quality and errors with respect to ideal machining. First the identification of the plane relating to the un-machined area (top surface) of the specimen is done for reference. This plane is then used for all subsequent measurements. The second step is the centring and alignment of the point cloud, and the selection of a strip, wide a half of the nominal tool diameter (0.2 mm) (Fig.4), comprising the reference plane, two faces of the pocket and the bottom base. This selection criterion is very important because it allows to perform the subsequent analysis without the effects of the fillet between the side surfaces. The last step foresees the fitting of the measurement points with ideal planes allowing an evaluation of local defects.

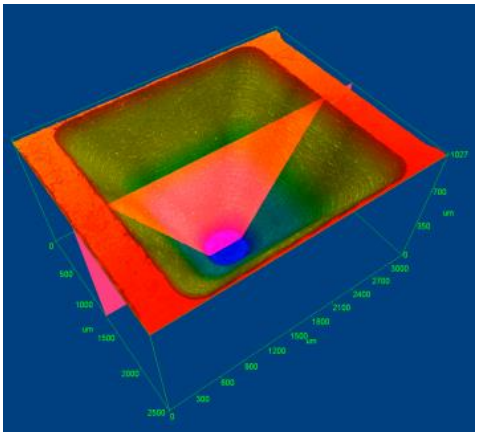

Fig. 3: Machined sloped pocket scanned by Axio CSM 700 confocal microscope.

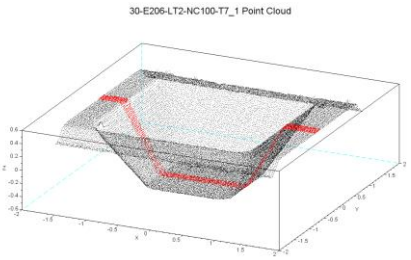

Fig. 4: Example of point cloud.

These two sets of measurements have different values and meaning: the former represents how the machine can detect the machining errors and consequently how it can mitigate them; the latter detects the real machining errors.

3. Experimental results and discussion

The experimental results show that different factors affect the machining performance. In particular, depth error and profile precision are influenced by energy level, control number, layer thickness, adjustment factors (Table 1) and workpiece material composition.

3.1. Depth error in relation to energy level, control number, layer thickness.

Fig. 5 shows the average depth errors measured for all cases reported in Table 1. From a first glance, some depth error trends show an overshoot in the first part of the machining. When the tool starts eroding the first layers, the process is not immediately stable and it also displays the occurrence of some short circuits. In this part of the process, the adjustment factor, is not adapted to the actual machining condition yet and it is more sensitive to the tool length measurement error (less than five measurement are considered for the update). As the erosion proceeds and if the electrical touches are more frequent, the adjustment factor finds its convergence, thus being capable of restoring an effective tool wear compensation. At higher depths, the depth error for all cases decreases and settles around ± 1 µm. However, for high CN and LT values, the depth error overshoot width shrinks independently of the energy level used in the processes. It is quite clear that the higher CN is, the smallest the depth error overshoot. Increasing LT means slower depth error convergence at higher depth. When LT passes from 1 to 2µm, no particular changes in the depth error behavior are observed.

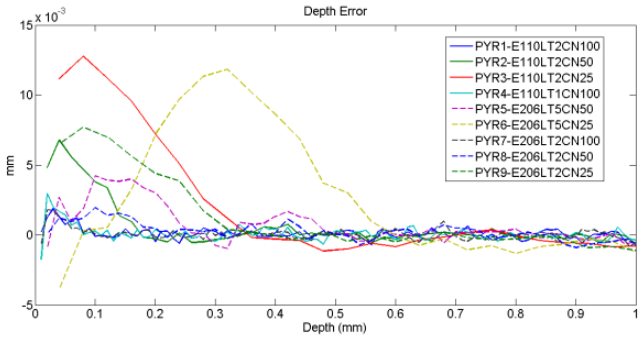

Fig. 5: Average depth error vs. depth for pyramids measured by Sarix SX 200.

The settling of the depth error around small values occurs at higher depths when E206 is used with respect to E110 and, in particular, this is verified for pyramids machined considering lower CN and higher LT values. As shown in Fig. 6, where the depth errors of pyramids 1 and 7 are reported, when CN is high and LT is small, energy level seems to have little effect on depth error behavior.

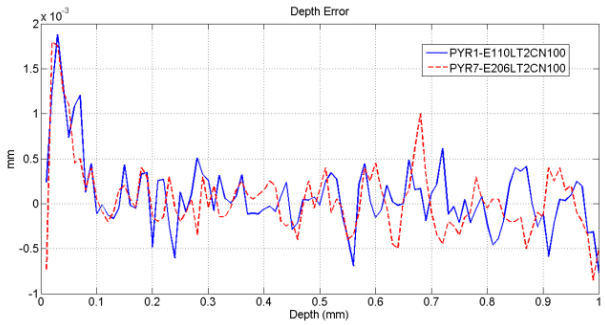

Fig. 6: Average depth error vs. depth for pyramids 1 and 7 measured by Sarix SX 200.

3.2. Depth error and tool wear in relation to initial adjustment factor variations.

In order to analyze the tool wear and put in evidence the effect on the performance induced by the adjustment factor, experiments related to pyr7 are considered in the following discussion. Along with the planned three replica, five more trials have been done using E206, CN = 100 and LT = 2µm. Fig. 7 reports the location of the machined pyramids. Different colours evidence the pyramids having better repeatability in terms of tool wear (blue) and worse repeatability (red). The features indicated by green and pink have been machined using higher and lower initial adjustment factors, respectively.

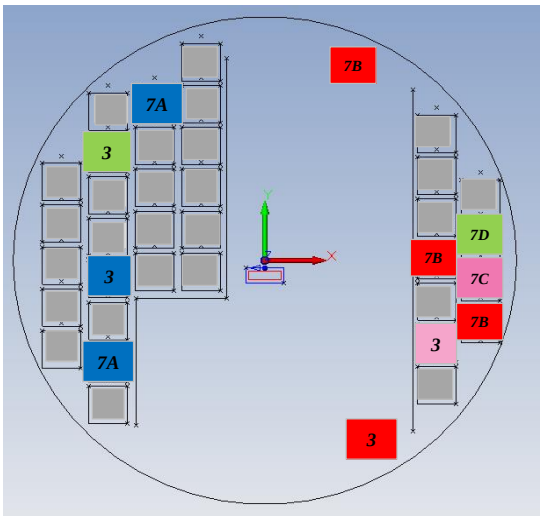

Fig. 7: Sample location of the pyramids pyr7 machined using E206, LT = 2µm and CN = 100 and pyr3 machined using E110, LT =2µm and CN = 25.

Fig. 8 shows the tool wear related to all pyr7 trials. The first two experiments (blue lines) display a relatively low tool consumption and high repeatability of the process, since the two lines have same slopes and are almost coincident. It is worth noticing that those features are machined in the same area of the workpiece.

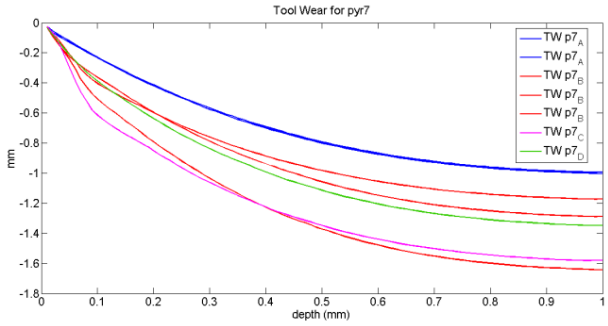

Fig. 8: Tool wear of pyramids machined using E206, LT = 2µm and CN = 100 (pyr7).

The red lines refer to the three pyramids machined in different parts of the workpiece (see Fig.7). In this case, the tool wear values and the line slopes are very dissimilar and a poor repeatability of the process can be detected. Moreover, the tool wear values recorded approximately up to 0.2 mm in depth have higher slopes with respect to the final part of the process, thus witnessing an unexpected higher tool consumption in the beginning of the erosion. A possible explanation to these peculiar trends can be ascribed to the material composition in the right part of the workpiece or to a modification of the surface induced by chemical reaction triggered by the erosion process. When the initial adjustment factor is decreased (pink line), the tool consumption is worse in the first part of the machining. On the contrary, when this value is decreased, the tool wear is more regular and lower. It is worth stressing that in general when the tool consumption at the beginning of the process is high, this negative trend is preserved along the machining, although in the final part of the process the tool wear behaviors settle at different values but with similar slopes.

The former observation about tool wear can be put in relation to depth error (Fig.9). When the tool wear is low, the initial depth error has positive and low value (blue lines). When the tool wear at the beginning of the machining is high, the related initial depth error is negative and a relevant overshoot is observed before it settles around small values. This phenomenon is detected for all considered cases, not only for pyr7. A negative initial depth error value leads to an increase of errors in the first part of the machining and to higher tool wear. Moreover, when the initial adjustment factor is decreased with respect to the previous cases (pink line), also depth error is hugely negative and immediately compensated by an intense positive overshoot. This means that at the beginning of the process, the erosion depth is far below the theoretical one. Hence, the control loop tried to minimize this error by increasing the adjustment factor and restoring the correct machining. When the adjustment factor is decreased (green line), the initial overshoot is strongly reduced and the depth error is immediately controlled.

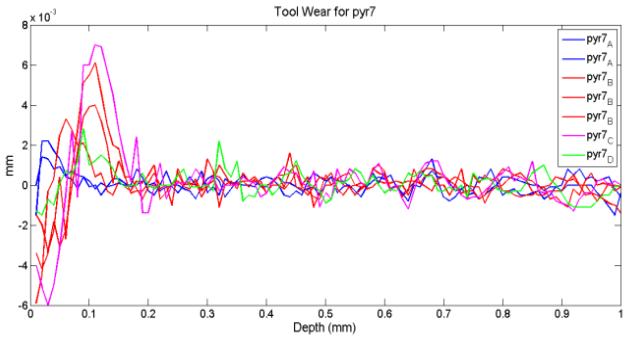

Fig. 9: Depth error vs. depth for pyramids machined using E206, LT = 2µm and CN = 100 (pyr7).

The same phenomena have been recorded for all the pockets with the same technological parameters confirming a different response of the process with respect to the sample area and a strong sensitivity of the process to the material composition. In order to prove this fact, the depth error related to all pyr3 experiments are reported in Fig. 10. Two trials, indicated by red and pink lines, respectively, behave in different way with respect the first two experiments and similarly between them. The position of the first and second pyramids related to the pyr3 parameter combination have been machined in the left part of the sample (A), the other two trials in the left part (B, see Fig. 2 for reference).

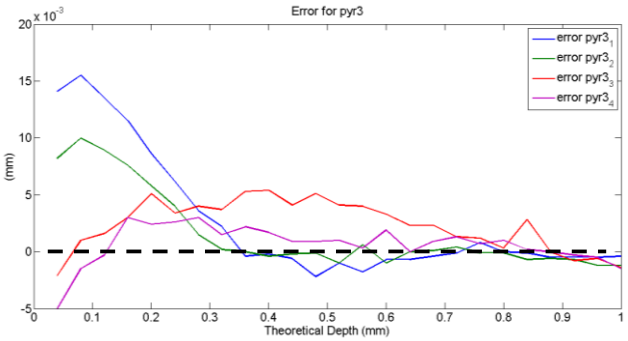

Fig. 10: Depth error vs. depth for pyramids machined using E110, LT = 2µm and CN = 25 (pyr3).

Fig. 11 shows the measurements of the layer depth error during machining. These quantities are calculated during the

additional control touches implemented in each part program besides those already foreseen by the standard routine. The additional control touches are obtained by operating an electrical touch in correspondence to the control point and another one at the center of pyramid bottom during the erosion process. The plots highlight two main issues: first, the layer depth error is generally negative, meaning that the tool has removed more material than the one expected.

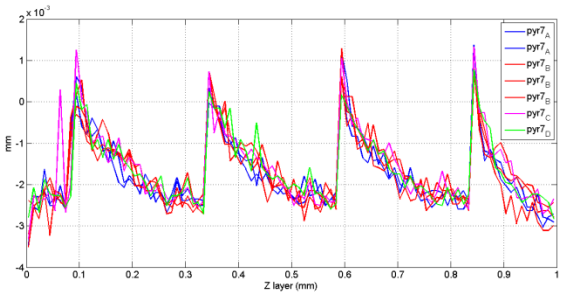

Fig. 11: Measurements of the difference between actual eroded and theoretical layer depths considering E206, LT = 2µm and CN = 100 (pyr7) .

Second, some spikes can be observed at same depths for all trials. These peaks occur in correspondence of the tool path changes due to the variation of the pyramid volume as the erosion proceeds. As clearly visible in Fig. 12, the size of squares covered by the tool path decreases as the eroded depth increases. After a square path in the pyramid center disappears, the layer depth error becomes positive, i.e. the tool has removed less material with respect to the expected value. This phenomenon is typical of the micro-EDM milling, where the eroded layer thickness is subject to variation also induced by the modification of tool path step-over.

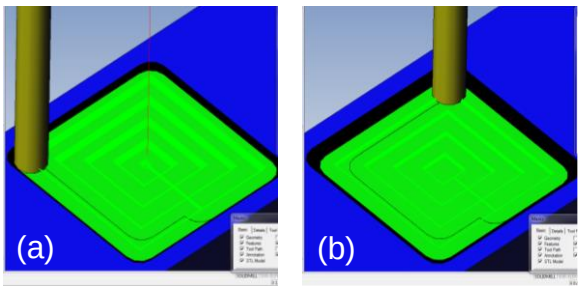

Fig. 12: example of tool path changes during pyramid machining: the central square disappears.

Fig. 13 shows that the average depth errors calculated during the additional control touches display similar behavior and values with respect to the standard measurements, except for the presence of the dips due to the former effect.

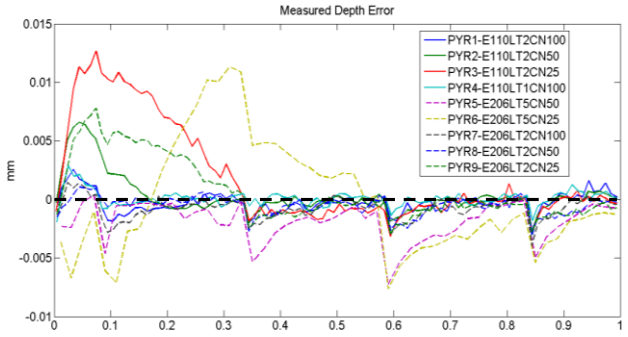

Fig. 13: Average depth error vs. depth for all pyramids measured by additional control touches.

3.3. Analysis of surface profiles using Axio CSM 700 microscope.

The machined features have been analysed using AXIO CSM 700 microscope. The acquired images have been then processed in order to obtain details about the actual inclination of the walls and quality of the surfaces. The following Fig. 14 displays an example of a transversal section of the acquired row including the machined pyramids, along with the fitting planes.

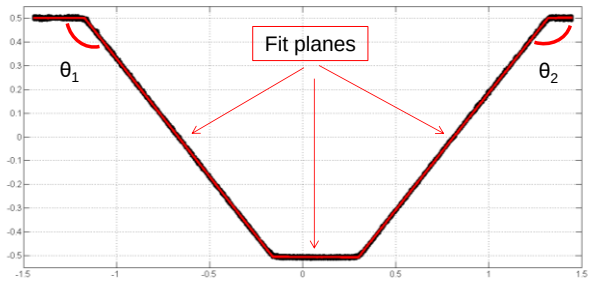

Fig. 14: transversal section of the pyramid pyr7_A: the red planes represent the fitting planes, θ1 and θ2 are the inclination angles of the walls.

Table 2 show the average distances between the fit plane and the actual bottom surface for each parameter combination used in the experiments. Generally, the machined pyramid depth is always higher than 1mm, which is the nominal value. Higher depths are detected in particular for the parameter combination pyr3.

Table 3 summarize other geometrical characteristics, such as the deviation of the draft angle from the nominal value (45°) and the errors and standard deviations related to the planes fitting the inclined walls. The actual draft angles θ_1 and θ_2 exhibit lower values with respect to the ideal one, though the difference is always less than 1°. As clearly visible, pyr3 and pyr6 display the worst performance in terms of draft angles and inclined walls. This fact is witnessed also by the close inspection of the walls, which reveal some surface irregularities. In particular, as shown in Fig. 15, the first trial related to pyr6 exhibits some surface deformations on the top of the features and in the bottom surface. This problem is detected for all trials of pyr6 and pyr3 and it is related to the initial process instability also witnessed by the depth error and tool wear, which are very high.

Table 2: Bottom plane fitting.

Pyramids	Bottom plane fit_min (mm)	Bottom plane fit_mean (mm)	Bottom plane fit_max (mm)
pyr1	0.9872	1.0058	1.0176
pyr2	0.9920	1.0074	1.0180
pyr3	0.9905	1.0072	1.0186
pyr4	0.9882	1.0071	1.0168
pyr5	0.9873	1.0047	1.0170
pyr6	0.9885	1.0048	1.0172
pyr7	0.9905	1.0059	1.0164
pyr7_c	0.9903	1.0054	1.0147
pyr7_d	0.9910	1.0072	1.0182
pyr8	0.9899	1.0049	1.0146
pyr9	0.9889	1.0046	1.0159

Table 3: angles, errors and standard deviation of the fitted planes with respect to the sloped walls for all considered cases.

Pyramids	Δθ1 (deg)	Δθ2 (deg)	err_sloped plane1	Std_sloped plane1	err_sloped plane2	Std_sloped plane2
pyr1	-0.2822	-0.3046	0.0092	0.0016	0.0091	0.0016
pyr2	-0.4624	-0.3543	0.0102	0.0018	0.0089	0.0016
pyr3	-0.6095	-0.4447	0.0114	0.0019	0.0104	0.0019
pyr4	-0.2854	-0.2255	0.0094	0.0017	0.0095	0.0016
pyr5	-0.5632	-0.2924	0.0108	0.0020	0.0107	0.0018
pyr6	-0.6666	-0.4088	0.0141	0.0024	0.0130	0.0024
pyr7	-0.3383	-0.1831	0.0102	0.0018	0.0113	0.0018
pyr7_c	-0.2361	-0.1176	0.0123	0.0021	0.0106	0.0019
pyr7_d	-0.2380	-0.1299	0.0098	0.0018	0.0103	0.0018
pyr8	-0.3795	-0.2866	0.0107	0.0020	0.0113	0.0020
pyr9	-0.5826	-0.3822	0.0102	0.0019	0.0103	0.0018

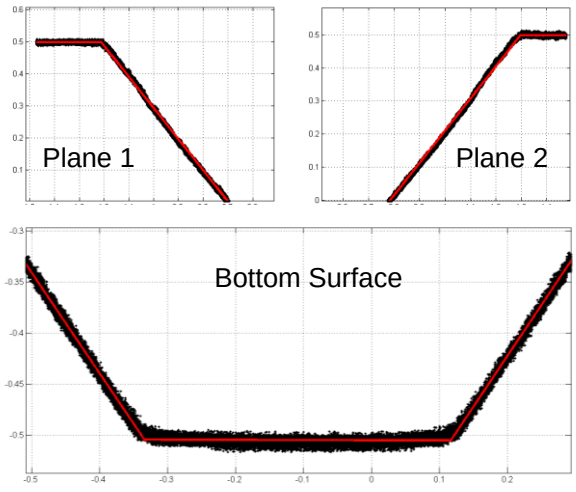

Fig. 15: inclined planes (1 and 2) and bottom surface related to pyr6 (first trials).

3.4. Material Removal Rate and machining times.

Table 4 reports the average values and standard deviations of the material removal rate (MRR) and machining times. The parameter combination pyr4, characterized by E110, LT = 1μm and CN = 100, is the slowest, since LT is small and CN is high, but MRR and machining times are almost the same for all trials. The fastest process is characterized by E206, LT = 5 μm and CN = 25 (pyr6), which on the contrary shows some problems in the machining times (very dissimilar values). This fact can be related to the previous observation about depth error. Indeed, as one can infer from Fig. 5, the curve related to pyr6 is the most peculiar, since the average depth error is relevant up to the middle of the machining. The parameter combination pyr5, characterized by E206, LT = 5 μm and CN = 50, exhibits the best MRR value among all trials and relatively small machining times. Considering same energy and layer thickness values, the increase of the control number does not provide any relevant variation in the machining times.

Table 4: MRR and machining times.

Pyramids	MRR_mean (mm^3/min)	MRR_STD	Machining Time_mean (s)	Machining Time_STD
pyr1	0.0336	$5.7*10^{-5}$	6496	25.186
pyr2	0.0337	0	5793.7	2.5166
pyr3	0.0338	$5.7*10^{-5}$	5417	4.3589
pyr4	0.211	0	9526.3	0.5774
pyr5	0.0887	$3.6*10^{-4}$	2352	9.5394
pyr6	0.0855	0.0055	2218.3	133.4516
pyr7	0.0428	$9.16*10^{-4}$	4853.8	84.8452
pyr7_c	0.042	-	4931	-
pyr7_d	0.0423	-	1932	-
pyr8	0.043	$6.25*10^{-4}$	4413.3	58.1062
pyr9	0.0439	0	4131.7	7.7369

4. Conclusions

The micro-EDM milling performance of sloped pockets (pyramids) having a draft angle equal to 45° realized in Si_3N_4-TiN ceramic composite has been analyzed in order to investigate the machining performance and surface profile errors. Two sets of measurements have been performed using Sarix SX 200 machine and Axio CSM 700 microscope. The preliminary experimental results comprising depth error measurements done by the micro-EDM machine suggest that the surface planarity of the sloped walls are affected by some defects found, in particular, on the top of the features. These errors are relevant when the control number is low, the layer thickness is high and the initial value of the adjustment factor is lower with respect to the expected one. When the depth error is high at the beginning of the process, also the tool wear is follows a negative trend, which is displayed in the first part of machining is preserved until the end of the process. When the initial depth error is low, the tool wear is lower. It has been also observed that the position of pyramids on the sample is of great importance. Indeed, using same parameter combination, a lack of repeatability has been detected for some trials. This is more likely due to a local material inhomogeneity rather than an effective troublesome machining. In terms of material removal rate, the best performance is obtained using high energy level and layer thickness. Considering same energy and layer thickness values, the increase of the control number does not provide any relevant variation in the machining times. The surface analysis of the machined feature performed using Axio CSM 700 microscope reveals good results. The angle values are very close to the ideal one (45°) and the errors calculated with respect to the ideal plane fitting are generally low.

Acknowledgements

The authors would like to thank ISTEC-CNR, Italy, for providing Si_3N_4-TiN samples. The authors acknowledge also the support of the Progetto Bandiera 'Fabbrica del Futuro', Sottoprogetto 2, Fab@Hospital.

References

[1] A. Bellosi et al., "Development and characterization of electroconductive Si_3N_4-TiN composite", J. Am. Cer. Soc. 1992; 83–93.

[2] M. Mazzocchi and A. Bellosi, "On the possibility of silicon nitride as a ceramic for structural orthopaedic implants. Part I: processing, microstructure, mechanical properties, cytotoxicity", J. Mat. Sci. Mat.

Med 2008; 19: 2881-7.
[3] K. Liu et al., “Process capabilities of micro-EDM and its applications”, Int. J. Adv. Manuf. Tech. 2010, 47:11-19.
[4] D. T. Pham et al., “Micro-EDM-recent developments and research issues”, J. Mat. Proc. Tech. 2004; 149(1-3): 50-57.
[5] B. Lauwers et al, “Investigation of the material removal mechanisms in EDM of composite ceramic materials”, J. Mat. Proc. Tech., 2004; 49/1-3:347-352.
[6] S. Clijsters et al, “EDM technology and strategy development for the manufacturing of complex parts in SiSiC”, J. Mat. Proc. Tech. 2010; 210: 631–641.
[7] C.C. Liu and J.-L-. Huang, “Effect of the electrical discharge machining on strength and reliability of TiN/Si_3N_4 composites”, Ceram. Int., 2007; 29: 679–687.
[8] Z.Y. Yu et al., “Micro-EDM for Three-dimensional Cavities—Development of Uniform Wear Method”, Annals of the CIRP, 1998; 47(1):169–172.
[9] G. Bissacco et al, “Towards the effective tool wear control in micro-EDM milling”, Int. J. Adv. Manuf. Tech. 2010; 47:3–9.
[10] F. Modica et al, “Study on depth error in fabrication of micro-channels via micro-EDM milling”, in Proc. ICOMM 2012, Evanston-Chicago (IL- USA).
[11] F. Modica, et al., “Machining of ceramic Si_3N_4-TiN scaffolds using micro-EDM”, in Proc. Promed 2012,Brescia, Italy, May 2-4, 2012.